

Further evidence for three-nucleon spin-orbit interaction in isotope shifts of $Z = \text{magic}$ nuclei

H. Nakada*

*Department of Physics,
Graduate School of Science, Chiba University,
Yayoi-cho 1-33, Inage, Chiba 263-8522, Japan*

and

Institut de Physique Nucléaire de Lyon, Université de Lyon 1, F-69622 Villeurbanne, France

(Dated: July 10, 2018)

It was pointed out [Phys. Rev. C **91**, 021302(R)] that the isotope shifts of the Pb nuclei, the kink at $N = 126$ in particular, can be well described by the Hartree-Fock-Bogolyubov calculations if a density-dependent LS interaction derived from the $3N$ interaction is incorporated. Effects of the density-dependence in the LS channel on the isotope shifts are extensively investigated for the Ca, Ni and Sn isotopes, using the semi-realistic M3Y-P6 interaction and its LS modified variant M3Y-P6a, as in the Pb case. It is found that almost equal charge radii between ^{40}Ca and ^{48}Ca are reproduced, as well as the isotope shifts in a long chain of the Sn nuclei, owing to the density-dependence in the LS channel. A kink is predicted at $N = 82$ for the isotope shifts of the Sn nuclei, in clear contrast to the interactions without the density-dependence.

PACS numbers: 21.10.Ft, 21.30.Fe, 21.60.Jz

I. INTRODUCTION

In the nuclear shell structure, which is formed by a series of the nucleonic single-particle (s.p.) orbits under the nuclear mean field (MF), the spin-orbit (ls) splitting plays an essential role. However, though known from the data, size of the ls splitting has been difficult to be accounted for only by the two-nucleon ($2N$) interaction [1]. Recent development of the chiral effective-field theory (χEFT) [2] indicates that the three-nucleon ($3N$) interaction gives significant density-dependence in an LS channel when it is converted to an effective $2N$ interaction [3, 4], and that this may account for the missing part of the ls splitting [4, 5].

There have been precise measurements on isotope shifts [6, 7]. As well as the ls splitting, they have supplied problems in nuclear structure theory that have not been solved for decades. As an important example, the isotope shifts of the Pb nuclei show a conspicuous kink at $N = 126$ when plotted as a function of the neutron number N . This kink was almost reproduced in a relativistic MF approach [8], though not in non-relativistic approaches with the Skyrme interactions. This difference has been recognized to originate from the isospin-dependence of the LS channels [9], and has led to extension of the Skyrme energy density functional [10]. The $n1g_{9/2}$ and $n0i_{11/2}$ s.p. levels are relevant to the kink at $N = 126$, which are nearly degenerate in the relativistic model and in the non-relativistic model with modified LS channels of Ref. [10]. However, such degeneracy is not observed in ^{209}Pb [11]. The author, together with a coauthor, pointed out that the density-dependence in the

LS channel enables us to reproduce the isotope shifts of the Pb nuclei fairly well, without degeneracy between the $n1g_{9/2}$ and $n0i_{11/2}$ orbitals [12]. This effect on the isotope shifts provides us with evidence for the $3N$ LS interaction that is practically independent of the ls splitting, suggesting a possibility that the two problems, origin of the ls splitting and the isotope shifts in Pb, are simultaneously solved by the $3N$ LS interaction. In this paper effects of the density-dependent LS channel are extensively examined for the isotope shifts of other $Z = \text{magic}$ nuclei.

Whereas a density-dependent LS interaction was argued in Ref. [13], motivated to account for the model-dependence of the isotope shifts in the Pb nuclei, primary origin of the difference between the relativistic and the Skyrme approaches has turned out to be the isospin-dependence of the LS channels. Since then the density-dependence in the LS channel has been considered only in a limited number of studies [14], and its influence on physical quantities other than energies has not been explored sufficiently.

II. FRAMEWORK

In the present work, the spherical Hartree-Fock-Bogolyubov (HFB) calculations are implemented for the Ca, Ni and Sn nuclei, as for Pb in Ref. [12]. Because the proton number Z is magic in these nuclei, it seems reasonable to investigate their systematic behavior in the spherical HFB regime, although there could be exceptions as will be mentioned below. The computational method is an extensive application of the Gaussian expansion method [15], and has been summarized in Ref. [16]. The effective Hamiltonian is comprised of the nuclear, Coulomb and center-of-mass (c.m.) parts:

* E-mail: nakada@faculty.chiba-u.jp

$H = H_N + V_C - H_{c.m.}$. The nuclear part H_N is taken to be non-relativistic and isoscalar, comprised of the central ($v^{(C)}$), LS ($v^{(LS)}$), tensor ($v^{(TN)}$), and the density-dependent central ($v^{(C\rho)}$), LS ($v^{(LS\rho)}$) channels for the $2N$ interaction, as well as of the kinetic energy term. In the former papers [17–19] $v^{(C\rho)}$ was denoted by $v^{(DD)}$. For $v^{(LS\rho)}$ the following form is assumed,

$$v_{ij}^{(LS\rho)} = 2i D[\rho(\mathbf{R}_{ij})] \mathbf{p}_{ij} \times \delta(\mathbf{r}_{ij}) \mathbf{p}_{ij} \cdot (\mathbf{s}_i + \mathbf{s}_j), \quad (1)$$

where $\mathbf{r}_{ij} = \mathbf{r}_i - \mathbf{r}_j$, $\mathbf{R}_{ij} = (\mathbf{r}_i + \mathbf{r}_j)/2$, $\mathbf{p}_{ij} = (\mathbf{p}_i - \mathbf{p}_j)/2$, $\rho(\mathbf{r})$ is the isoscalar nucleon density and \mathbf{s}_i is the spin operator, with i and j being indices of constituent nucleons. V_C contains the exchange terms without approximation and $H_{c.m.}$ consists both of one- and two-body terms.

The Michigan-three-range-Yukawa (M3Y) interactions were obtained from the G -matrix [20]. By modifying the M3Y-Paris interaction [21] phenomenologically, the semi-realistic M3Y- Pn interactions have been developed [19, 22], whose density-independent terms $v^{(X)}$ ($X = C, LS$ and TN) are expressed by the Yukawa function. Responsible for the shell structure, the ls splitting is significant to describing nuclear structure. Except M3Y-P6a, $v^{(LS)}$ has been enhanced from that of the original M3Y-Paris interaction, to reproduce s.p. level sequence in the absence of $v^{(LS\rho)}$. With keeping the tensor channels $v^{(TN)}$ of the M3Y-Paris interaction, Z - or N -dependence of the shell structure is obtained reasonably well, as exemplified by the level inversion of $p0d_{3/2}$ and $p1s_{1/2}$ from ^{40}Ca to ^{48}Ca [24]. Among several parameter-sets, it has been found that M3Y-P6 gives prediction of magic numbers compatible with most available experimental data, in wide range of the nuclear chart including unstable nuclei [25]. Here M3Y-P6 is taken as a yardstick for investigating effects of the $3N$ LS interaction. The values of the parameters [26] in M3Y-P6 have been given in Ref. [19].

The χ EFT derives density-dependence in the LS channel as an effect of the $3N$ interaction [4, 5], which may complement the $2N$ LS interaction with respect to the ls splitting. Based on this χ EFT indication, $v^{(LS\rho)}$ has been introduced in Ref. [12], instead of enhancing $v^{(LS)}$, which yields a variant of the M3Y-P6 interaction called M3Y-P6a. However, since the currently available χ EFT is not yet convergent at $\rho \gtrsim \rho_0$, where ρ_0 denotes the saturation density, the χ EFT results have not completely been followed in quantitative respect. The functional $D[\rho]$ is taken to be

$$D[\rho(\mathbf{r})] = -w_1 \frac{\rho(\mathbf{r})}{1 + d_1 \rho(\mathbf{r})}. \quad (2)$$

The d_1 term of the denominator, which has been fixed to be 1.0 fm^3 in M3Y-P6a, is employed to avoid instability for increasing density, whereas the results are not sensitive to d_1 as will be shown in Sec. III. Since the effective interactions have been more or less adjusted to the observed ls splitting, size of the ls splitting should not change much even when the density-dependence is taken

into account. Therefore the remaining parameter w_1 has been fitted to the splitting of the $n0i$ orbits obtained with M3Y-P6 at ^{208}Pb [12]. This M3Y-P6a interaction will be applied to other $Z = \text{magic}$ nuclei. Note that all the parameters of M3Y-P6a except in $v^{(LS)}$ and $v^{(LS\rho)}$ are identical to those of M3Y-P6.

Since $v^{(LS\rho)}$ in Eq. (1) has zero range, its contribution to the total energy can be represented by a functional of local currents. The particle-hole terms, which appear in the Hartree-Fock (HF) regime, are summarized as

$$\begin{aligned} E_{ph}^{(LS\rho)} = \frac{1}{4} \int d^3r D[\rho(\mathbf{r})] \left\{ \rho(\mathbf{r}) \nabla \cdot \mathbf{J}(\mathbf{r}) + \sum_{\tau=p,n} \rho_\tau(\mathbf{r}) \nabla \cdot \mathbf{J}_\tau(\mathbf{r}) \right. \\ \left. + i \mathbf{J}(\mathbf{r}) \cdot \mathbf{j}^*(\mathbf{r}) + i \sum_{\tau=p,n} \mathbf{J}_\tau(\mathbf{r}) \cdot \mathbf{j}_\tau^*(\mathbf{r}) \right. \\ \left. - i \mathbf{J}^*(\mathbf{r}) \cdot \mathbf{j}(\mathbf{r}) - i \sum_{\tau=p,n} \mathbf{J}_\tau^*(\mathbf{r}) \cdot \mathbf{j}_\tau(\mathbf{r}) \right. \\ \left. - \mathbf{Q}(\mathbf{r}) \cdot \boldsymbol{\sigma}(\mathbf{r}) - \sum_{\tau=p,n} \mathbf{Q}_\tau(\mathbf{r}) \cdot \boldsymbol{\sigma}_\tau(\mathbf{r}) \right\}, \quad (3) \end{aligned}$$

where the density $\rho(\mathbf{r})$ and the other local currents are defined by

$$\begin{aligned} \rho(\mathbf{r}) &= \sum_{\tau=p,n} \rho_\tau(\mathbf{r}), \quad \rho_\tau(\mathbf{r}) = \sum_{\alpha,\beta \in \tau} \varrho_{\alpha\beta} \phi_\beta^\dagger(\mathbf{r}) \phi_\alpha(\mathbf{r}), \\ \mathbf{j}(\mathbf{r}) &= \sum_{\tau=p,n} \mathbf{j}_\tau(\mathbf{r}), \quad \mathbf{j}_\tau(\mathbf{r}) = -i \sum_{\alpha,\beta \in \tau} \varrho_{\alpha\beta} \phi_\beta^\dagger(\mathbf{r}) \nabla \phi_\alpha(\mathbf{r}), \\ \mathbf{Q}(\mathbf{r}) &= \sum_{\tau=p,n} \mathbf{Q}_\tau(\mathbf{r}), \quad \mathbf{Q}_\tau(\mathbf{r}) = i \sum_{\alpha,\beta \in \tau} \varrho_{\alpha\beta} \nabla \phi_\beta^\dagger(\mathbf{r}) \times \nabla \phi_\alpha(\mathbf{r}), \\ \boldsymbol{\sigma}(\mathbf{r}) &= \sum_{\tau=p,n} \boldsymbol{\sigma}_\tau(\mathbf{r}), \quad \boldsymbol{\sigma}_\tau(\mathbf{r}) = 2 \sum_{\alpha,\beta \in \tau} \varrho_{\alpha\beta} \phi_\beta^\dagger(\mathbf{r}) \mathbf{s} \phi_\alpha(\mathbf{r}), \\ \mathbf{J}(\mathbf{r}) &= \sum_{\tau=p,n} \mathbf{J}_\tau(\mathbf{r}), \quad \mathbf{J}_\tau(\mathbf{r}) = 2i \sum_{\alpha,\beta \in \tau} \varrho_{\alpha\beta} \phi_\beta^\dagger(\mathbf{r}) \mathbf{s} \times \nabla \phi_\alpha(\mathbf{r}), \end{aligned} \quad (4)$$

with the s.p. basis function $\phi_\alpha(\mathbf{r})$ and the one-body density matrix $\varrho_{\alpha\beta} = \langle \Phi | a_\beta^\dagger a_\alpha | \Phi \rangle$ for the HF or HFB state $|\Phi\rangle$. It should be noticed that, because of the presence of $D[\rho]$, integration by parts does not simplify the expression of $E_{ph}^{(LS\rho)}$.

Under the spherical symmetry, $\mathbf{Q}_\tau(\mathbf{r}) = \boldsymbol{\sigma}_\tau(\mathbf{r}) = 0$, $i[\mathbf{j}_\tau(\mathbf{r}) - \mathbf{j}_\tau^*(\mathbf{r})] = \nabla \rho_\tau(r)$ and $\mathbf{J}_\tau(\mathbf{r}) = \mathbf{J}_\tau^*(\mathbf{r}) = (\mathbf{r}/r^2) \sum_{\alpha,\beta \in \tau} \varrho_{\alpha\beta} \phi_\beta^\dagger(\mathbf{r}) (2\boldsymbol{\ell} \cdot \mathbf{s}) \phi_\alpha(\mathbf{r})$ with $\boldsymbol{\ell} = \mathbf{r} \times \mathbf{p}$ (ϕ_α, ϕ_β are postulated to be spherical bases). $E_{ph}^{(LS\rho)}$ yields the ls potential as follows [27]:

$$-\frac{1}{r} \left[D[\rho(r)] \frac{d}{dr} (\rho(r) + \rho_\tau(r)) + \frac{1}{2} \frac{\delta D}{\delta \rho} [\rho(r)] (\rho(r) + \rho_\tau(r)) \frac{d\rho(r)}{dr} \right] \boldsymbol{\ell} \cdot \mathbf{s}. \quad (5)$$

The same Hamiltonian is applied to the pairing channels in the HFB calculations, including the two-body term of $H_{c.m.}$. Since $D[\rho(\mathbf{r})]$ does not contain the pairing tensor, contribution of $v^{(LS\rho)}$ to the pair energy is represented analogously to that given in Ref. [28].

The semi-realistic M3Y-P6a [12] interaction is primarily used in this work, and its results are compared with those of M3Y-P6 [19] to exhibit effects of the density-dependence in the LS channel. As mentioned above, the strength parameter w_1 in M3Y-P6a has been determined so as to equate the $n0i$ splitting at ^{208}Pb to its counterpart in M3Y-P6. This makes influence on other ls splitting insignificant as well. For instance, the $n0d$ splitting at ^{40}Ca decreases merely by 4% if replacing M3Y-P6 by M3Y-P6a. The equal-filling approximation [29] is applied to odd- N nuclei, whose ground states have one quasiparticle. It should be noted that the results of M3Y-P6 are qualitatively similar to those of the other interactions that lack density-dependence in the LS channels. To show it, the Gogny-D1M interaction [30] will be taken as an example, which has successfully been applied to describing structure of many nuclei. While calculations beyond the spherical HFB have been implemented with D1M and other globally fitted interactions, qualitative improvement over the spherical HFB regime has not been reported so far on the isotope shifts of the nuclei under investigation, to my best knowledge.

III. RESULTS AND DISCUSSIONS

The frequency difference of corresponding atomic de-excitations among isotopes is converted to the difference in mean-square (m.s.) charge radii of nuclei. Hence the isotope shifts are expressed by the m.s. charge radius of a certain nuclide relative to that of a reference nuclide with equal atomic number Z . The m.s. charge radius of the AZ nucleus is given by

$$\langle r^2 \rangle_c(^AZ) = \langle r^2 \rangle_p(^AZ) + \langle r^2 \rangle_c(p), \quad (6)$$

where $\langle r^2 \rangle_p(^AZ)$ represents the m.s. radius for point-proton distribution in AZ and $\langle r^2 \rangle_c(p)$ the charge m.s. radius of a single proton. By subtracting the c.m. contribution, $\langle r^2 \rangle_p(^AZ)$ is obtained as

$$\langle r^2 \rangle_p(^AZ) = \frac{1}{Z} \sum_{i \in p} \langle \Phi | (\mathbf{r}_i - \mathbf{R})^2 | \Phi \rangle. \quad \left(\mathbf{R} = \frac{1}{A} \sum_i \mathbf{r}_i \right) \quad (7)$$

Because $\langle r^2 \rangle_c(p)$ is canceled out, the isotope shift is denoted by $\Delta \langle r^2 \rangle_p(^AZ) = \langle r^2 \rangle_p(^AZ) - \langle r^2 \rangle_p(^{A_0}Z)$ in this paper, with ^{A_0}Z taken as a reference.

A. Pb isotopes, revisited

It is customary to define the isotope shift of the Pb nuclei by adopting ^{208}Pb as a reference, $\Delta \langle r^2 \rangle_p(^APb) = \langle r^2 \rangle_p(^APb) - \langle r^2 \rangle_p(^{208}\text{Pb})$. As has been shown by comparing the M3Y-P6 and M3Y-P6a results in Ref. [12], the isotope shifts of the Pb nuclei can be improved with the density-dependent LS interaction.

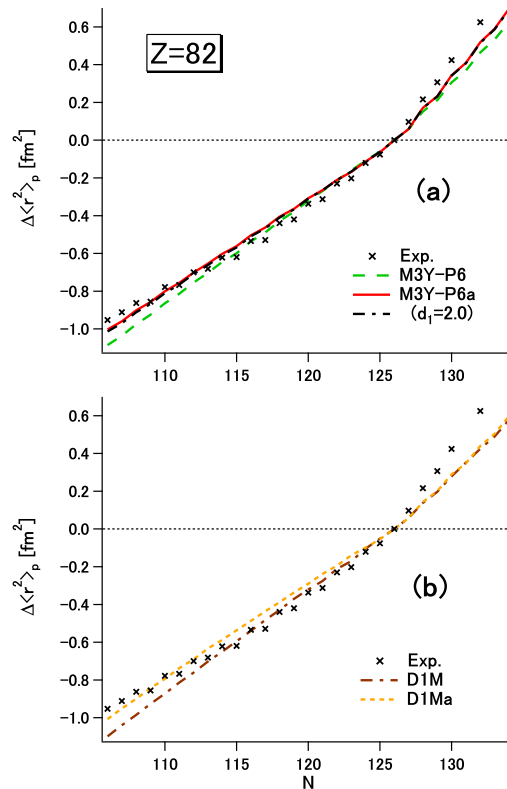


FIG. 1. (Color online) Isotope shifts of the Pb nuclei $\Delta \langle r^2 \rangle_p(^APb)$ obtained from the HFB calculations. (a) Comparison among the results with M3Y-P6 (green dashed line), M3Y-P6a (red solid line) and its variant of $d_1 = 2.0 \text{ fm}^3$ (black dot-dashed line). (b) Comparison between the results with D1M (brown dot-dashed line) and D1Ma (orange short-dashed line). Experimental data quoted from Ref. [31] are shown by crosses for reference.

It is exhibited in Fig. 1(a) that the d_1 parameter in Eq. (2), which has been presumed to be 1.0 fm^3 in M3Y-P6a, hardly influences the results. If d_1 is assumed to be 2.0 fm^3 , $w_1 = 842 \text{ MeV} \cdot \text{fm}^8$ follows by equating the $n0i$ splitting to that with M3Y-P6 at ^{208}Pb , instead of $742 \text{ MeV} \cdot \text{fm}^8$ in M3Y-P6a. Notice that $D[\rho_0]$ values are close to each other. The results with $d_1 = 2.0 \text{ fm}^3$ are shown by the black dot-dashed line. Comparison to the results with M3Y-P6a confirms insensitivity to d_1 .

The density-dependent LS term in the effective interaction may produce different behavior in the isotope shift unless it is too weak, as typically represented by the kink at $N = 126$ in $\Delta \langle r^2 \rangle_p(^APb)$. This is not constrained to the M3Y-P6 case, although it depends on the interaction to certain degree how strong its effects are. It is here illustrated by D1M. The LS channel of the D1M interaction is obtained if $D[\rho]$ in $v^{(\text{LS}\rho)}$ is replaced by a constant w_0 . The strength of $v^{(\text{LS})}$ (i.e. w_0) was determined in a fully phenomenological manner. When $v^{(\text{LS}\rho)}$ is introduced, it is reasonable to reduce w_0 so as to keep size of the ls splitting, which leaves the ratio $w_1\rho_0/w_0$ almost arbi-

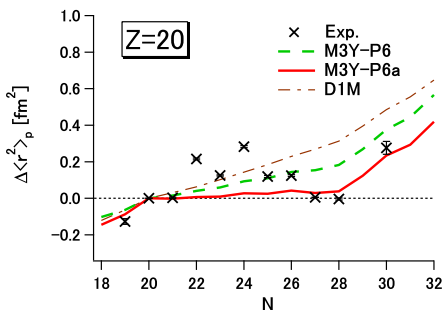


FIG. 2. (Color online) Isotope shifts of the Ca nuclei $\Delta\langle r^2 \rangle_p(^A\text{Ca})$, obtained from the HFB calculations with M3Y-P6a (red solid line), in comparison to those with M3Y-P6 (green dashed line) and D1M (thin brown dot-dashed line). Experimental data are quoted from Ref. [31] (crosses).

trary. To see qualitative effects of $v^{(\text{LS}\rho)}$, w_0 is reduced to 30% of its original value and w_1 is adjusted by equating the $n0i$ splitting to that of the original D1M, with taking $d_1 = 1.0 \text{ fm}^3$. This interaction is called D1Ma in the present article. The results of D1Ma on the isotope shifts of the Pb nuclei are compared to the D1M results in Fig. 1(b). The experimental data are shown for reference, although comparison to them is not the point here. As has been pointed out [10, 32], the slope of the isotope shifts becomes steeper in $N > 126$ than in $N \leq 126$ because of the occupation on $n0i_{11/2}$. With D1M (D1Ma), $n1g_{9/2}$ lies lower than $n0i_{11/2}$ by 1.4 MeV (1.2 MeV) in ^{208}Pb . This energy difference suppresses occupation on $n0i_{11/2}$ near ^{208}Pb , and therefore the effect of the density-dependent LS interaction is hindered in $N > 126$, though present. However, because the $n0i_{13/2}$ function shrinks, the isotope shift varies more slowly with D1Ma than with D1M in $N \leq 126$, producing a visible kink at $N = 126$.

B. Ca isotopes

The isotope shifts of the Ca (*i.e.* $Z = 20$) nuclei are defined by taking ^{40}Ca as a reference nuclide, $\Delta\langle r^2 \rangle_p(^A\text{Ca}) = \langle r^2 \rangle_p(^A\text{Ca}) - \langle r^2 \rangle_p(^{40}\text{Ca})$. The HFB results are depicted and compared with the data in Fig. 2. It is commented that the weak instabilities against the octupole [17, 19] and the pairing [25] correlations in ^{40}Ca are lifted with M3Y-P6a. The inversion of the $p0d_{3/2}$ and $p1s_{1/2}$ levels from ^{40}Ca to ^{48}Ca is reproduced with M3Y-P6a as well as with the previous interactions [24], in which $v^{(\text{TN})}$ plays a significant role.

As doubly magic nuclei, both ^{40}Ca and ^{48}Ca are expected to be well described within the HF regime. Although it has been known that their charge radii are close to each other, this property has been difficult to be reproduced by self-consistent nuclear structure calculations so far. It is interesting to see $\Delta\langle r^2 \rangle_p(^{48}\text{Ca}) \approx 0$, *i.e.* $\langle r^2 \rangle_p(^{40}\text{Ca}) \approx \langle r^2 \rangle_p(^{48}\text{Ca})$, in the M3Y-P6a result. Attraction from the neutrons occupying $0f_{7/2}$ determines

$\Delta\langle r^2 \rangle_p(^{48}\text{Ca})$. As illustrated for $n0i$ orbits in Fig. 1 of Ref. [12], the density-dependence in the LS channel tends to shrink the $j = \ell + 1/2$ orbits while extends the $j = \ell - 1/2$ orbits. Therefore the m.s. radius of neutrons occupying the $0f_{7/2}$ orbit comes smaller, decreasing by 0.23 fm^2 at ^{40}Ca when M3Y-P6 is switched to M3Y-P6a. Moreover, the m.s. radius of $n0f_{7/2}$ increases from ^{40}Ca to ^{48}Ca only by 0.035 fm^2 with M3Y-P6a, in contrast to 0.365 fm^2 with M3Y-P6. This is interpreted as the neutrons on $0f_{7/2}$ feel mutual attraction and the density-dependent LS channel blocks them to distribute more broadly, which further suppresses $\langle r^2 \rangle_p$. These effects lead to the result $\Delta\langle r^2 \rangle_p(^{48}\text{Ca}) \approx 0$. Thus it may be possible to ascribe the very small difference in the charge radii between ^{40}Ca and ^{48}Ca to an effect of the $3N$ interaction.

Though not shown to keep the figure visible, the density-dependence in the LS channel makes $\Delta\langle r^2 \rangle_p(^{48}\text{Ca})$ smaller also when switching D1M to D1Ma, confirming the qualitative effect of the density-dependence. In quantitative respect, however, $\Delta\langle r^2 \rangle_p(^{48}\text{Ca})$ with D1Ma is close to that with M3Y-P6, mainly because D1M gives almost twice larger $\Delta\langle r^2 \rangle_p(^{48}\text{Ca})$ than M3Y-P6.

The isotope shifts of $^{42-46}\text{Ca}$ show sizable deviation from those of $^{40,48}\text{Ca}$. Since $\langle r^2 \rangle_p(^A\text{Ca})$ varies almost linearly from ^{40}Ca to ^{48}Ca in the spherical HFB calculations, none of the interactions including M3Y-P6a reproduce the observed N -dependence of $\Delta\langle r^2 \rangle_p(^A\text{Ca})$ in $N = 22 - 26$. This discrepancy may be ascribed to effects beyond MF, including influence of the α -clustering. On the contrary, the rising of $\Delta\langle r^2 \rangle_p(^A\text{Ca})$ from ^{48}Ca to ^{50}Ca in the M3Y-P6a result is in good agreement with the data, while not so good in the M3Y-P6 and D1M results. This also supports presence of the density-dependent LS interaction.

C. Ni isotopes

For the Ni (*i.e.* $Z = 28$) isotopes ^{60}Ni is used as a reference, defining isotope shifts as $\Delta\langle r^2 \rangle_p(^A\text{Ni}) = \langle r^2 \rangle_p(^A\text{Ni}) - \langle r^2 \rangle_p(^{60}\text{Ni})$. The results are depicted in Fig. 3.

Steeper slope is obtained for $\Delta\langle r^2 \rangle_p(^A\text{Ni})$ with M3Y-P6a than with M3Y-P6 in $28 \leq N \leq 40$. This is attributed to contribution of neutrons occupying $n0f_{5/2}$, which distribute more broadly when the density-dependence is incorporated in the LS channel. Compared to M3Y-P6, M3Y-P6a gives slightly better agreement with the measured value for ^{58}Ni while slightly worse for ^{64}Ni . Since both of the M3Y-P6 and M3Y-P6a results are in reasonable agreement with the existing data, it is not obvious to tell whether the density-dependent LS channel improves the theoretical results on $\Delta\langle r^2 \rangle_p(^A\text{Ni})$ or not. It is desired to measure neutron-rich or neutron-deficient isotopes, *e.g.* ^{56}Ni .

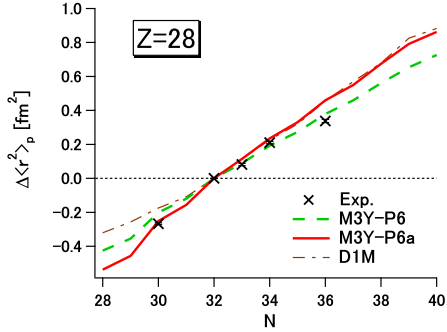


FIG. 3. (Color online) Isotope shifts of the Ni nuclei $\Delta\langle r^2 \rangle_p(^A\text{Ni})$. See Fig. 2 for conventions.

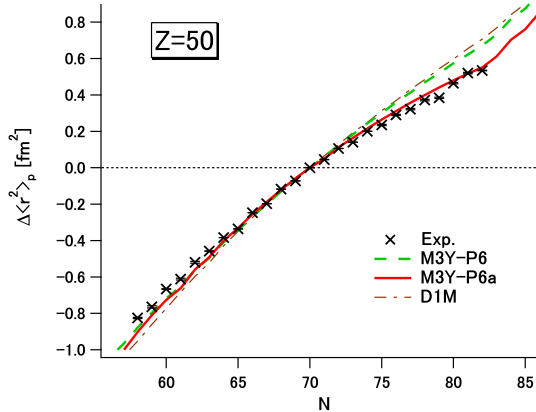


FIG. 4. (Color online) Isotope shifts of the Sn nuclei $\Delta\langle r^2 \rangle_p(^A\text{Sn})$. See Fig. 2 for conventions.

D. Sn isotopes

For the Sn (*i.e.* $Z = 50$) isotopes ^{120}Sn is adopted as a reference nuclide, by which isotope shifts are defined as $\Delta\langle r^2 \rangle_p(^A\text{Sn}) = \langle r^2 \rangle_p(^A\text{Sn}) - \langle r^2 \rangle_p(^{120}\text{Sn})$. The results are presented in Fig. 4.

It is found that $\Delta\langle r^2 \rangle_p(^A\text{Sn})$ is well described with M3Y-P6a in a long chain of the Sn isotopes, owing to the density-dependence in the LS channel. The density-dependence gives narrower distribution of neutrons occupying the $0h_{11/2}$ orbit, whose attraction reduces $\Delta\langle r^2 \rangle_p(^A\text{Sn})$ in $N > 70$. The same trend is obtained with D1Ma.

It is remarked that a kink is predicted at $N = 82$ with the M3Y-P6a interaction. Origin of this kink is accounted for analogously to the Pb case. Attraction from neutrons occupying $0h_{9/2}$ contributes to the broader proton distribution. While occupation probability on $n0h_{9/2}$ is negligibly small in $N \leq 82$, $n0h_{9/2}$ is partially occupied in $N > 82$ owing to the pairing correlation, although the lowest s.p. level above $N = 82$ is $n1f_{7/2}$. The relatively large m.s. radius of $n0h_{9/2}$, for which the density-dependence in the LS channel is responsible, produces the kink at $N = 82$. The reduction of the radii in

TABLE I. Root-m.s. charge radii of the reference nuclei. Spherical HFB results with M3Y-P6 and M3Y-P6a are compared with experimental data [31]. (μp) and (ep) corresponds to the data on $\langle r^2 \rangle_c(p)$.

nuclide		M3Y-P6	M3Y-P6a	Exp.
^{16}O	(μp)	2.732	2.725	2.6991 ± 0.0052
	(ep)	2.743	2.737	
^{40}Ca	(μp)	3.491	3.487	3.4776 ± 0.0019
	(ep)	3.500	3.496	
^{60}Ni	(μp)	3.825	3.779	3.8118 ± 0.0016
	(ep)	3.834	3.787	
^{120}Sn	(μp)	4.653	4.627	4.6519 ± 0.0021
	(ep)	4.659	4.634	
^{208}Pb	(μp)	5.493	5.464	5.5012 ± 0.0013
	(ep)	5.499	5.470	

$N < 82$, an effect of the density-dependent LS channel on $n0h_{11/2}$, makes the kink more conspicuous. This kink in $\Delta\langle r^2 \rangle_p(^A\text{Sn})$ at $N = 82$ is a clear contrast to the results of M3Y-P6 and D1M which have no density-dependent LS channel. Thus the density-dependence in the LS channel is essential to the kink. Future measurements with respect to this kink (*i.e.* $\Delta\langle r^2 \rangle_p(^A\text{Sn})$ beyond $N = 82$) will be intriguing, which could be a touchstone of the 3N LS effects.

E. Absolute values of charge radii and neutron-skin thickness

Although the isotope shifts are the main subject of this paper, it deserves discussing absolute values of the charge radii of the reference nuclei as well. While the finite-size effects of protons are canceled out in the isotope shifts, absolute values of the charge radii are affected by the ambiguity in the charge radius of an isolated proton. A recent compilation [33] gives two values, $\langle r^2 \rangle_c(p) = 0.84087 \pm 0.00039$ by μp Lamb shift and 0.8775 ± 0.0051 by ep CODATA. The spherical HFB results on the root-m.s. charge radii $\sqrt{\langle r^2 \rangle_c(^AZ)}$ with M3Y-P6 and M3Y-P6a are tabulated in Table I, obtained from Eq. (6) by taking both of the μp and the ep values for $\langle r^2 \rangle_c(p)$, in comparison to the experimental data [31].

It is found via comparison of the M3Y-P6a results to the M3Y-P6 ones that the density-dependence in the LS channel tends to reduce the radii. Whereas this effect is weak in ^{16}O and ^{40}Ca which are so-called LS-closed nuclei, it is stronger in ^{60}Ni , ^{120}Sn and ^{208}Pb , with $0.02 - 0.05$ fm difference between the two interactions. It is reasonable that the effect is minimal in the LS-closed nuclei in which all the ls partners (the $j = \ell \pm 1/2$ orbitals) are filled, in contrast to the jj -closed nuclei in which there is a pair of an occupied $j = \ell + 1/2$ and unoccupied $j = \ell - 1/2$ orbitals. Since the parameters of the central channels have been more or less fitted to the measured radius of ^{208}Pb , the charge radius is well reproduced with M3Y-P6 for this nucleus, and so for ^{120}Sn . This indicates that M3Y-P6a slightly underestimates the charge radii of ^{120}Sn and ^{208}Pb , although it gives values

closer to the measured ones than M3Y-P6 for ^{16}O and ^{40}Ca . As the MF approaches are expected to be the more appropriate for the heavier nuclei, there may be a room to readjust the parameters in the central channels. Such readjustment could influence the saturation density by 1%.

The neutron-skin thickness, which is usually represented by the difference of the neutron and proton root-m.s. radii $\sqrt{\langle r^2 \rangle_n} - \sqrt{\langle r^2 \rangle_p}$ in a single nucleus, attracts interests because it correlates to variation of the symmetry energy for increasing density [34]. Because of their neutron excess and of experimental accessibility, the neutron-skin thickness is frequently argued for ^{48}Ca , ^{68}Ni , ^{132}Sn and ^{208}Pb . The density-dependence in the LS channel hardly influences this quantity at ^{208}Pb and at ^{132}Sn ; difference between M3Y-P6 and M3Y-P6a is 0.001 fm or less. On the other hand, $\sqrt{\langle r^2 \rangle_n} - \sqrt{\langle r^2 \rangle_p}$ is larger by 0.011 fm with M3Y-P6a than with M3Y-P6 at ^{68}Ni and smaller by 0.014 fm at ^{48}Ca . This is because the effects of the density-dependence tend to be canceled if both of the ls partners are occupied. Though not very strong, influence of the density-dependence in the LS channel cannot be discarded for certain nuclides in order to argue their neutron-skin thickness to 0.01 fm accuracy.

IV. SUMMARY

Effects of the density-dependent LS interaction, which was suggested from the chiral $3N$ interaction, have been extensively studied on the isotope shifts of the Ca, Ni and Sn nuclei. Since the density-dependence makes the LS interaction stronger in the nuclear interior relative to its exterior, the s.p. wave functions of the $j = \ell + 1/2$ orbits shrink while those of the $j = \ell - 1/2$ orbits become broader, if the ls splitting is maintained. It was pointed out in the previous paper that, owing to this mechanism, the kink in the isotope shifts of the Pb nuclei at $N = 126$ can be better described by introducing the density-

dependent LS channel.

The spherical HFB calculations have been implemented with M3Y-P6a, which contains density-dependence in the LS channel but is identical to M3Y-P6 in the other channels. It is found that almost equal charge radii between ^{40}Ca and ^{48}Ca have been described well, although this property has been difficult to be reproduced in the MF calculations so far. Moreover, the isotope shifts of the Sn nuclei are in excellent agreement with the available data. A kink is predicted at $N = 82$ in the isotope shifts of Sn, in contrast to those obtained from interactions with no density-dependent LS channel. Future experiments on the isotope shifts of Sn beyond $N = 82$ are awaited, as well as on ^{56}Ni for which predictions significantly depend on interactions.

Absolute values of the charge radii have also been argued. The density-dependence in the LS channel reduces the absolute values, amounting to about 1% except for the LS-closed nuclei. The density-dependence may influence the neutron-skin thickness in ^{48}Ca and ^{68}Ni by about 0.01 fm. Both are small but not necessarily negligible.

ACKNOWLEDGMENTS

The author is grateful to J. Margueron for discussions. This work is financially supported in part as Grant-in-Aid for Scientific Research on Innovative Areas, No. 24105008, by The Ministry of Education, Culture, Sports, Science and Technology, Japan, and as Grant-in-Aid for Scientific Research (C), No. 25400245, by Japan Society for the Promotion of Science. Numerical calculations are performed on HITAC SR16000s at Institute of Management and Information Technologies in Chiba University, Information Technology Center in University of Tokyo, Information Initiative Center in Hokkaido University, and Yukawa Institute for Theoretical Physics in Kyoto University.

-
- [1] K. Andō and H. Bandō, *Prog. Theor. Phys.* **66**, 227 (1981).
 - [2] E. Epelbaum, W. Glöckle and U.-G. Meißner, *Nucl. Phys. A* **747**, 362 (2005).
 - [3] N. Kaiser, *Phys. Rev. C* **68**, 054001 (2003).
 - [4] M. Kohno, *Phys. Rev. C* **86**, 061301(R) (2012).
 - [5] M. Kohno, *Phys. Rev. C* **88**, 064005 (2013).
 - [6] P. Aufmuth, K. Heilig and A. Steudel, *At. Data Nucl. Data Tables* **37**, 455 (1987).
 - [7] I. Angeli, *At. Data Nucl. Data Tables* **87**, 185 (2004).
 - [8] M.M. Sharma, G. Lalazissis and P. Ring, *Phys. Lett. B* **317**, 9 (1994).
 - [9] M.M. Sharma, G. Lalazissis, J. König and P. Ring, *Phys. Rev. Lett.* **74**, 3744 (1995).
 - [10] P.-G. Reinhard and H. Flocard, *Nucl. Phys. A* **584**, 467 (1995).
 - [11] R.B. Firestone *et al.*, *Table of Isotopes*, 8th edition (John Wiley & Sons, New York, 1996).
 - [12] H. Nakada and T. Inakura, *Phys. Rev. C* **91**, 021302(R) (2015).
 - [13] J.M. Pearson and M. Farine, *Phys. Rev. C* **50**, 185 (1994).
 - [14] S. Goriely, *Nucl. Phys. A* **933**, 68 (2015).
 - [15] E. Hiyama, Y. Kino and M. Kamimura, *Prog. Part. Nucl. Phys.* **51** (2003) 223.
 - [16] H. Nakada, *Nucl. Phys. A* **808**, 47 (2008).
 - [17] H. Nakada, *Phys. Rev. C* **78**, 054301 (2008).
 - [18] H. Nakada, *Phys. Rev. C* **81**, 027301 (2010).
 - [19] H. Nakada, *Phys. Rev. C* **87**, 014336 (2013).
 - [20] G. Bertsch, J. Borysowicz, H. McManus and W.G. Love, *Nucl. Phys. A* **284**, 399 (1977).
 - [21] N. Anantaraman, H. Toki and G.F. Bertsch, *Nucl. Phys.*

- A **398**, 269 (1983).
- [22] H. Nakada, Phys. Rev. C **68**, 014316 (2003).
- [23] H. Nakada, Phys. Rev. C **81**, 051302(R) (2010).
- [24] H. Nakada, K. Sugiura and J. Margueron, Phys. Rev. C **87**, 067305 (2013).
- [25] H. Nakada and K. Sugiura, Prog. Theor. Exp. Phys. **2014**, 033D02.
- [26] The unit of $t_\rho^{(\text{SE})}$ ($t_\rho^{(\text{TE})}$) in Table I of Ref. [19] should be corrected to MeV fm^6 (MeV fm^4).
- [27] There was an error in Eq. (5) in Ref. [12], which should be multiplied by the factor 2.
- [28] J. Dobaczewski, H. Flocard and J. Treiner, Nucl. Phys. A **422**, 103 (1984).
- [29] S. Perez-Martin and L.M. Robledo, Phys. Rev. C **78**, 014304 (2008); N. Schunck *et al.*, Phys. Rev. C **81**, 024316 (2010).
- [30] S. Goriely, S. Hilaire, M. Girod and S. Pèru, Phys. Rev. Lett. **102**, 242501 (2009).
- [31] I. Angeli and K.P. Marinova, At. Data Nucl. Data Tables **99**, 69 (2013).
- [32] P.M. Goddard, P.D. Stevenson and A. Rios Phys. Rev. Lett. **110**, 032503 (2013).
- [33] K.A. Olive *et al.* (Particle Data Group), Chin. Phys. C **38**, 090001 (2014).
- [34] M. Centelles, X. Roca-Maza, X. Viñas and M. Warda, Phys. Rev. Lett. **102**, 122502 (2009).